Influence of contact interface morphology on the nonlinear interaction between a longitudinal wave and a contact interface with friction : A numerical study

Abdelkrim Saidoun, Anissa Meziane, Mathieu Renier, Fan Zhang, Henri Walaszek

Version of Record: https://www.sciencedirect.com/science/article/pii/S0165212520303164
Manuscript_3c95efb1105c25b1fedbe8553fd40990

Influence of contact interface morphology on the nonlinear interaction between a longitudinal wave and a contact interface with friction : A numerical study

Abdelkrim Saidoun[a], Anissa Meziane[b], Mathieu Renier[b], Fan Zhang[a], Henri Walaszek[a]

[a] *CETIM, Senlis, France*
[b] *Univ. Bordeaux, CNRS, Arts et Metiers Paris Tech, Bordeaux INP, I2M, UMR 5295, F-33400, Talence, France.*

Abstract

The detection and evaluation of closed cracks are of prime interest in industry. Whereas conventional ultrasonic methods fail to detect these defects, nonlinear methods based on activation of the nonlinear behavior of closed cracks constitute an interesting alternative. The aim of this article is to give a better understanding of interactions between cracks and a longitudinal elastic wave for a quantitative investigation into nonlinear signatures. Using a 1D approach based on the literature, the nonlinear signature of the contact interface is analyzed in two cases. In the first, the interface is initially open and in the second, it is initially closed before interaction with an elastic wave. These signatures were qualitatively observed experimentally in real cracks. Next, in order to investigate the influence of the coexistence of open and closed zones within the interface, a numerical 2D-study is proposed. Two configurations are considered involving two steel blocks in contact, with different contact interface morphologies. The first configuration is a perfectly plane contact interface, while the second one involves an interface between a concave surface and a plane surface. A non-plane wave is also considered. This study attempts to establish a link between local second harmonic generation and interface parameters (pre-stress, gap) that can be exploited for the nondestructive quantitative evaluation of interfaces or cracks.

1. Introduction

The evaluation of damage at an early stage of fracture is relevant in many industrial applications such as aeronautics or nuclear plants. Ultrasonic methods based on linear wave scattering are efficient for detecting defects and for characterizing material elasticity, but are less sensitive to micro-cracks or closed cracks. In this context, nonlinear acoustics constitutes a good alternative for detection and evaluation of these defects, taking advantages of the nonlinear behavior of contact dynamics induced by an acoustic wave if its amplitude activates sufficiently nonlinear contact behavior.

When elastic waves and contact interfaces interact, specific nonlinear acoustic phenomena can be observed [1] : DC-effect, subharmonics generation or hysteresis/storage effects, etc. These non-classical effects are due to complex contact behavior: an asymmetrical normal stiffness, the presence of asperities and multiphysical interactions on contact surfaces that result in specific contact acoustic nonlinearity (CAN). In order to exploit these nonlinear effects it is essential to understand the complex interactions between waves and contact interfaces, and this can be achieved using analytical and numerical models. As it is not possible to include the whole complexity of contact interfaces in a model, the contact effects and study methodology have to be carefully chosen according to the objectives of the study.

Previous studies have investigated the effect of contact nonlinearity on nonlinear acoustic signatures by considering phenomenological contact models [2][3][4]. They lead to a mean stress/strain relation that is able to describe the observed nonlinear behavior. The advantage of these approaches is that observed behavior can be described, however they do not make it possible to understand the physical behavior of interfaces. Other approaches, called the "physical models", based on physical contact behavior have been used to investigate the nonlinear interaction of waves and contact interfaces [5][6]. Aleshin *et al.* included the influence of asperities on nonlinear acoustics [7] [8], in a model based on memory-diagrams which has been implemented in a Finite Element (FE) code.

Richardson [9] provides an analytical study of the interaction between a longitudinal plane wave (therefore infinite) and an infinite contact interface between two identical media considering a unilateral contact law. It corresponds to an infinitely rigid contact that cannot support tension and hence opens up in the tension phase [9]. In the case of an incident sinusoidal wave, second harmonic generation efficiency (which corresponds to the ratio of the second harmonic to the incident wave amplitude) can be determined, and shows a specific nonlinear signature. Based on this work, other studies aimed at explaining the relation between contact nonlinearity and harmonic evolution considering an interface [10][11][12][13] or a crack [6]. They show that nonlinear signatures provide some information on interface parameters (contact stresses, friction induced energy dissipation, crack orientation, etc.) if they are measurable. These studies take into account both the "clapping" effect and sliding with friction on a perfectly plane interface. They give a good understanding of interactions between wave and contact in a model case, but do not take into account asperities and non-conforming profiles that actually exists in the case of real cracks and that can play an important role during dynamic interactions with waves.

Including asperities in the model leads to difficulties of interpretation if too many parameters are involved. For example, in [7], the contact model introduces a nonlinear normal contact stiffness in compression, and consequently other effects are introduced during the interactions between waves and contact interfaces that, as far as we know, are not fully analyzed and understood. The present paper considered non-conforming profile interface between two deformable solids. A unilateral contact law with Coulomb's friction is applied locally in order to investigate the effect of the coexistence of open and closed zones in the interaction zone. This is physical approaches to contact modeling. If it does not take into account a large number of contact effects (adhesion, asperities, contact stiffness, wear), but

it describes interface closing/opening ("clapping" effect) and sliding with friction ("sliding" effect) with only one parameter: the friction coefficient. In the first part of the paper, a 1D model of the nonlinear interaction between a plane wave and an infinite interface is used to analyze second harmonic evolution as a function of pre-stress and incident wave magnitude in the cases of closed and open contact interfaces. Next, the experimental results of second harmonic evolution as a function of applied stress on a real crack are presented. In the third part, the effect of the coexistence of closed and open parts within the interaction zone on second harmonic generation is investigated numerically using a 2D-FE model. Investigation of local contact behavior in relation to local harmonic generation is a way to go further in the evaluation of cracks and contact interfaces.

2. 1D-Numerical study of a longitudinal wave reflected from a unilateral contact interface

In this part, a homogeneous, isotropic elastic half-space defined as Ω is assumed to be in perfect contact with a rigid wall on a line Γ_c at $x = 0$. The half-space and the rigid plane are brought into contact under a given compression normal stress σ_0 ($\sigma_0 < 0$) or maintained open with a normal initial displacement gap u_0 ($u_0 < 0$) (Figure 1). An incident plane longitudinal wave is generated at $x = -L$ and propagates linearly in Ω in the positive x-direction with a velocity c_L (approximately 6000 m.s^{-1} in steel). A unilateral contact law is considered at the interface. Assuming a large enough incident amplitude, "clapping" (alternative opening and closing) can occur and thus affects the reflected wave nonlinearly.

With these assumptions, a 1D model of the wave propagation and reflection from the interface is valid. Equation (1) governs wave propagation:

$$\frac{\partial^2 u}{\partial t^2} - c_L^2 \frac{\partial^2 u}{\partial x^2} = 0 \quad , \text{ in } \Omega \tag{1}$$

where $u(t, x)$ refers to the displacement in the $\mathbf{x}$ direction.

The initial conditions at $t = 0$ represent the unperturbed state in the half-space ($x < 0$). When the interface is closed, a uniform pre-stress ($\sigma_0 \leq 0$) is applied to the semi-infinite medium Ω. The incident plane wave is associated with a normal stress and displacement in Ω. Denoting σ_n and u_n respectively normal stress and displacement at interface ($x = 0$), the normal unilateral contact law can be written including σ_0 and u_0:

$$\begin{cases} \sigma_n + \sigma_0 \leq 0 \\ u_n + u_0 \leq 0 \\ (\sigma_n + \sigma_0)(u_n + u_0) = 0 \\ \sigma_0 u_0 = 0 \end{cases} \tag{2}$$

The first equation states that only a compression stress can be applied to the interface. The normal stress σ_n is allowed to be positive although the crack is closed as long as $\sigma_n \leq \mid \sigma_0 \mid$. The second line corresponds to the non-penetration condition. In the case of an initially open interface ($u_0 \leq 0$), u_n can be positive and the crack remain open as long as $u_n \leq \mid u_0 \mid$. The third line corresponds to a complementary equation, indicating that the contact interface is neither open nor closed. The last condition indicates that initially the interface is either closed or open.

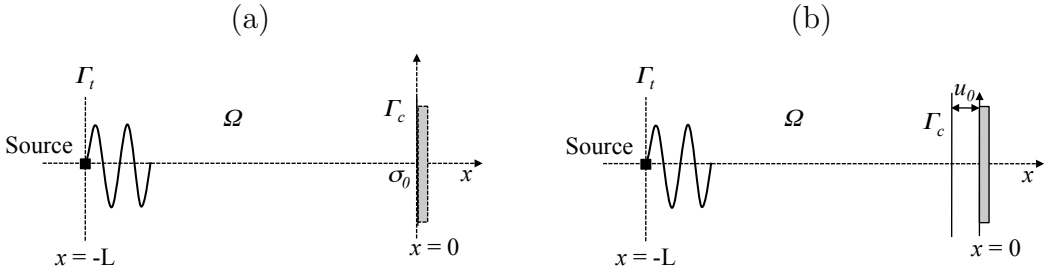

Figure 1: System considered for 1D-study of the interaction between a normal incidence longitudinal wave and a contacting interface: (a) initially closed interface with a normal compression stress $\sigma_0 \leq 0$ (gap $u_0 = 0$) and (b) initially open contact interface with normal gap $u_0 \leq 0$ ($\sigma_0 = 0$).

As demonstrated in [9], the solution at the interface can easily be obtained analytically

or semi-analytically for a harmonic incident wave. In the present work, a numerical solution using a finite difference scheme is preferred for its flexibility in particular for a tone burst incident waveform. The numerical scheme is very similar to that presented in [14]. The wave equation is solved in time using the classic second order finite difference approach. A transparent boundary condition is defined at Γ_t. The wave equation (1) is discretized in Ω using the classic Euler finite difference scheme. In the following results, the simulation is run at 0.7 Current-Friedrich-Lewy condition (CFL) and the space discretization is $\delta x = \lambda_{2\omega}/24$ where $\lambda_{2\omega}$ is the wavelength of the second harmonic. The values of the numerical parameters were checked to ensure the convergence of the numerical solution through grid size and time step.

The incident wave is a five cycle sinusoidal signal modulated by a Taper window (central frequency 1 MHz). Figure 2(a) illustrates the solution at $x = -L$ for a closed interface ($\sigma_0 < 0$), showing the incident and the reflected wave. As $\sigma_{inc} \geq \mid \sigma_0 \mid$, "clapping" is activated and the reflected wave is distorted. Incident and reflected waves are then windowed and converted to frequency domain using a FFT (Fast Fourier Transform) (Figure 2(b)). As expected, the reflected wave spectrum contains higher harmonics due to the nonlinear behavior at contact interface.

In the following, the evolution of the second harmonic in the reflected wave is studied for both open and closed interfaces. The part of the spectrum that corresponds to the second harmonic is filtered and transformed back to the time domain using an IFFT (Inverse FFT). Second harmonic magnitude A_2 is extracted from the envelope of the filtered temporal signal. It is then normalized using the incident wave magnitude, defining second harmonic efficiency as $\eta = \frac{A_2}{u_{inc}}$.

In the case of an initially closed interface, the condition for "clapping" to be activated is that maximum magnitude of incident stress exceeds the absolute value of σ_0 ($\sigma_{inc} \geq \mid \sigma_0 \mid$). If

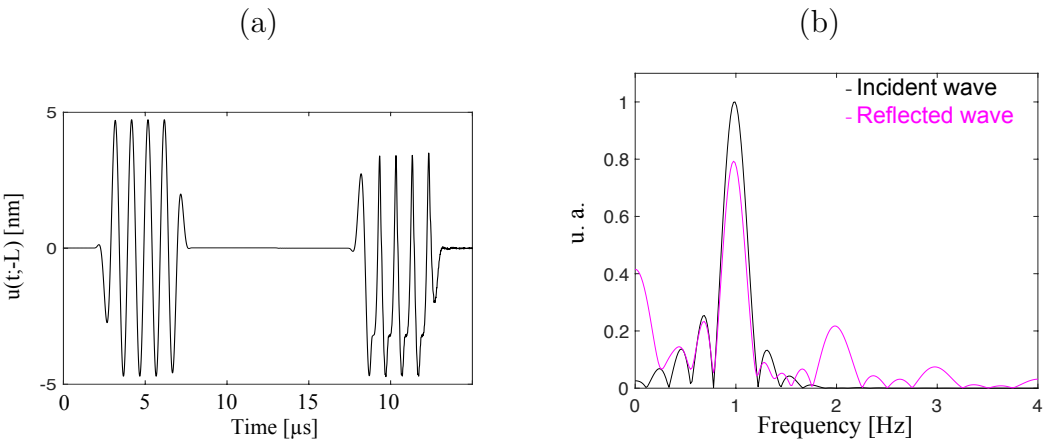

Figure 2: Numerical results for a closed interface with $\sigma_0 = -1.4$ MPa. The incident wave is a Taper windowed 5-cycle longitudinal wave of maximal magnitude $u_{inc} = 5$ nm which corresponds to $\sigma_{inc} = 3$ MPa. (a) Displacement at x=-L and (b) the associated spectrum for the incident and reflected waves. The spectrum is normalized using the incident harmonic amplitude A_{inc}.

not, the interface stays closed all the time, giving rise to a linear behavior of the interface and no harmonics will appear in the reflected wave spectrum. As in [9], a dimensionless parameter $\xi \geq 0$ is defined as the ratio of initial pre-stress to maximum magnitude of incident wave:

$$\xi = \frac{\mid \sigma_0 \mid}{\sigma_{inc}} \tag{3}$$

In the case of an initially open interface, the condition for "clapping" to be activated is that maximum magnitude of incident displacement at the interface exceeds absolute value of the initial gap u_0 ($u_{inc} \geq \mid u_0 \mid$). Otherwise, the interface will stay open all the time and behave as a linear reflector. Thus, a dimensionless parameter $\psi \geq 0$ can be defined as :

$$\psi = \frac{\mid u_0 \mid}{u_{inc}} \tag{4}$$

Figure 3 shows the evolution of harmonic efficiency η as a function of ξ and ψ, for a closed and open interface respectively. In both cases, there is nonlinearity for $(\xi; \psi) \in [0; 1]^2$. In the case of a closed crack, the second harmonic efficiency exhibits a maximum value for $\xi = 0.35$, corresponding to a configuration of maximum "clapping" [9]. For an initially open

interface, η decreases as ψ increases. As expected, η is greater in the case of a closed interface and the point $\xi = 0$ and $\psi = 0$ corresponds to the same case where the interface is in perfect contact: $u_0 = 0$ and $\sigma_0 = 0$. To explain these evolutions, it should be remebered that harmonic efficiency is linked to the distortion of the incident wave due to the intermittent closing and opening of the interface. The numerical solution for an initially open interface shows that after one or two intermittent of openings and closings (depending on u_0), the interface remains open during the rest of the contact/wave interaction. This explains why the harmonic efficiency η decreases as ψ increases. For the case of an initially closed interface, when ξ increases, the duration of the closed state of the interface increases gradually. Thus for a value of ξ between 0 and 0.35, this has the effect of increasing η. Then for values of ξ between 0.35 and 1, the interface then switches to a mainly closed configuration, with fewer and fewer opening phases. Consequently, η decreases to 0 for the extreme case of a completely closed interface $\xi = 1$. As the evolutions of η are different for open and closed interfaces, they constitute specific acoustic signatures, which could be exploited to determine qualitatively the state of the interfaces. It can be noticed that the amplitude of η is not perfectly equal to 0 for $\xi > 1$ and $\psi > 1$. These observed non-zero values of η for values of σ_0 or u_0 that would provide a linear behavior is explained by the presence of sidelobes on the spectrum, leading to a non-zero value of the second harmonic amplitude. Nevertheless, this amplitude value can be considered negligible.

3. Experimental evidence of different evolutions of the second harmonic for a real fatigue crack

In this section, experimental results are presented for the second harmonic generation of a real fatigue crack. The experimental set-up and cracked sample are shown in Figure 4 (a) and (b) respectively. Compression force loading is applied to the sample using a threaded rod and nuts. This force is monitored through a load-cell located between the screw thread

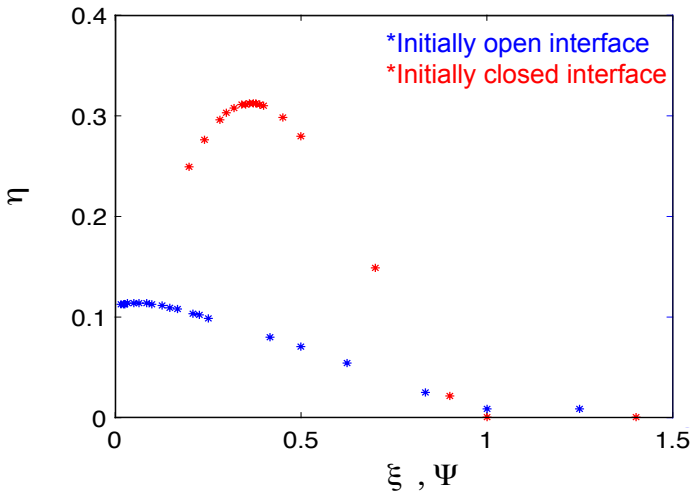

Figure 3: Second harmonic efficiency η as a function of dimensionless parameters ξ and ψ for initially closed and open interface respectively.

and the sample. In practice the system is mounted horizontally to allow the application of loads lower than the sample weight. A 32 mm diameter broadband longitudinal transducer of center frequency 1 MHz (V102, Panametrics, Waltham, MA, USA) sends a tone burst from the left-hand side. A 2 MHz transducer (V104, Panametrics, Waltham, MA, USA) is used as a receiver on the right-hand side of the sample. The input signal is generated by a wave generator (33120A, Agilent Tec., Santa Clara, CA, USA) and the received signal is measured on an oscilloscope (LT224, Lecroy, Chestnut Ridge, NY, USA) with both communicating with the computer over a GPIB interface. The excitation signal sent to the transducer is a 10-cycle tone burst with a Taper window which is amplified (GA-2500A, Ritec Inc., Warwick, RI, USA). The number of cycles and the window of the excitation signal were chosen to maximize the value of the second harmonic generated by contact nonlinearity and to enable the separation of echoes in the sample. The cracked sample is a non-normalized CT-specimen designed especially for this study (Figure 4 (b)). An open crack was created by fatigue test ($R = \sigma_{min}/\sigma_{max} = 0.1$, with a frequency of 5 Hz and a maximum force of 47 kN). An extensometer indicated a crack length of 44 mm during the test. Four positions

were considered for the transmitter and the receiver (Figure 4 (b)) for the study: including wave propagation through cracked zones for two configurations (zone 1 and zone 2). The third zone is a priori away from the crack and the fourth zone is an undamaged reference zone.

The amplitude of the incident longitudinal wave at the interface is of prime importance for the results, as shown in section 2, see equations 3 and 4. In this configuration, it is not possible to measure incident wave magnitude at the interface, but it was measured on the left edge of the sample in zone 4 (Figure 4(b)), supposed to be flawless. For this measurement, the sample is unloaded. The source is the same as in Figure 4. The displacement amplitude is measured on the free surface of the sample (i.e transmitted through the flawless part of the sample) using a laser vibrometer (OFV 353, Polytec, Waldbronn, Germany). In this configuration, the maximum measured displacement is 28 nm. Thus assuming that both absorption and beam spreading are neglectable, the incident wave displacement amplitude is equal to 14 nm in the sample and the associated normal incident stress amplitude equal to 4 MPa.

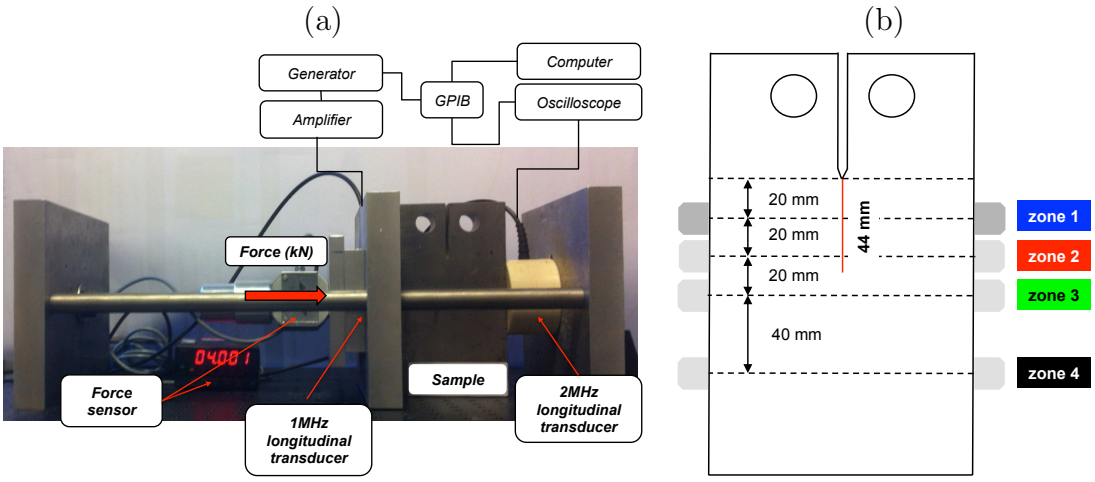

Figure 4: (a) Experimental set-up and (b) cracked sample scheme showing the four zones of study (dotted lines) and the fatigue crack (red line).

The experimental procedure consists in increasing normal load while the amplitude of the

incident wave is maintained constant at its highest level. In order to ensure reproducibility of measurements, the sample is subjected to ten loading-unloading cycles prior to ultrasonic measurements to ensure more stable contact conditions at the crack interface. Measurements for increasing forces are repeated three times for each configuration (zone of measurement), each time removing and replacing both transducers. Springs that applied constant stress on both transducers ensure reproducible generation and measurement conditions. Figure 5 shows temporal signals and associated spectra for a 2 kN load for each zone. As expected, the amplitude of the signal transmitted through the sample is maximal for zone 4 (with no crack). In the cracked zone, the amplitude of the signal increases from zone 1 to zone 3, indicating that the crack is open and certainly more open from the notch to the edge of the crack. In the frequency domain, the level of the second harmonic (-40 dB) is the same in zone 3 and 4, indicating that this is probably due mainly to classical material nonlinearity. The second harmonic reaches -22 dB for zone 2 and -28 dB for zone 1, indicating that a contact nonlinearity is activated in these zones.

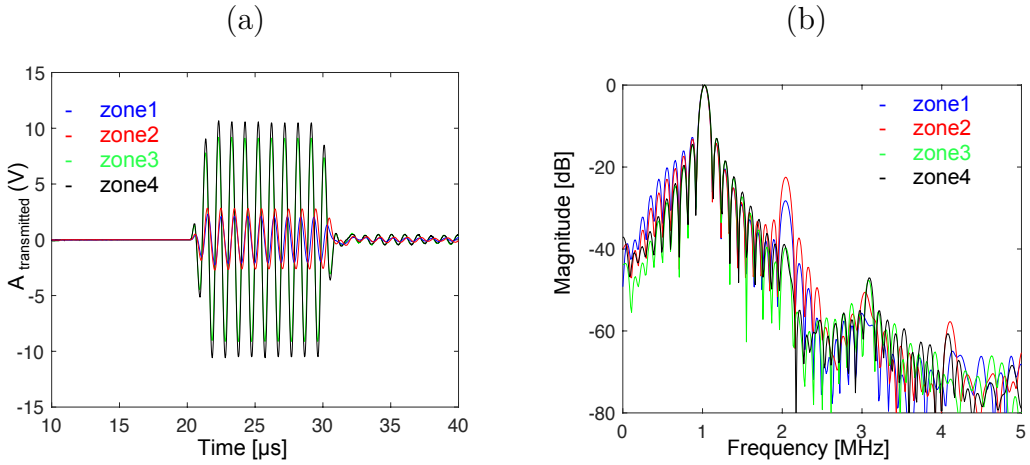

Figure 5: (a) Received time signals and (b) corresponding normalized FFT in dB for the 4 zones and an applied force of 2 kN.

To obtain the signatures of previous analyses (in section 2) experimentally, the normal load is gradually increased. If the interface is initially open, increasing normal load has the

effect of decreasing the initial gap $\mid u_0 \mid$ and thus the parameter ψ. In the case of an initially closed interface, an increasing the normal load will increase normal contact stress $\mid \sigma_0 \mid$ and the parameter ξ. Experimentally, second harmonic efficiency is defined as the ratio of the second harmonic measured by the receiver transducer to the maximal signal value received on zone 4 (far from the crack). Figure 6 shows the evolution of second harmonic efficiency ($\eta_{exp} = A_2/A_{inc-zone4}$) as a function of the applied force for the four zones (1-4) of study.

First, for zones 3 and 4, η_{exp} does not depend on applied force, thus confirming that nonlinearity comes mainly from material nonlinearity. For zone 1, η_{exp} remains quite low but increases slowly with the increasing load until it reaches an almost constant value. This evolution of η_{exp} qualitatively follows the signature of an open interface for a decreasing initial gap $\mid u_0 \mid$. Finally, for zone 2, η_{exp} values are higher and its evolution shows an undeniable maximum for a load of 3.3 kN, as in the signature of a closed interface in section 2 for an increasing ξ.

Experimental results highlight different evolutions of the second harmonic efficiency depending on the location of the transducers and suggest that they may be related to the general behavior of the interface: open interface and closed interface, which might be described numerically with a unilateral contact law. This law, describing elementary behaviors of opening and closing of the interfaces, associated to a 1D-description of the problem appears to be able to provide acoustic signatures which are qualitatively similar to the experimental results.

Nevertheless, when considering real cracks, assumptions made for this numerical model are strong: asperities in contact, non-plane interface morphology, different contact effects are not taken into account and can explain differences in measured A_2 magnitudes and evolutions versus applied load. In the literature, more realistic models are proposed to take into account these different aspects, asperities for instance [3][7], but the unilateral aspect is generally lost, which means that a weak but non-zero stress is generally applied in traction.

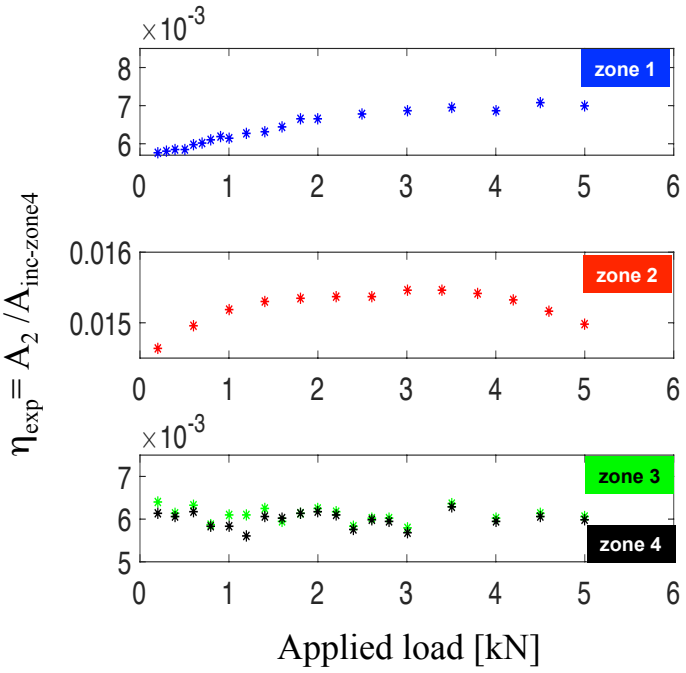

Figure 6: Experimental second harmonic efficiency η_{exp} as a function of applied force for the four studied zones. Experimentally, the second harmonic efficiency is defined as the ratio of the second harmonic measured by receiver transducer to the maximal value of signal received on the fourth zone (far from the crack)

Supplementary parameters are needed to describe the contact interface. In this paper, we take into account the fact that the interface includes open and closed zones while keeping a unilateral contact law. In this way the number of parameters for the study is kept low. Thus, in the following, a numerical analysis of the influence of the interface morphology on the second harmonic evolution is proposed, keeping the same contact law. In the zone of interaction between contact interface and longitudinal wave, coexisting open and closed parts will both contribute to the nonlinear distortion of transmitted wave. By applying an external compression load, the contact configuration and the interface morphology will evolve and may result in modifications to the second harmonic efficiency.

4. 2D-Numerical study of a longitudinal wave interacting with contact interfaces of different morphologies

Two configurations (Figure 7) are considered both including two steel blocks in contact. They differ in their contact interface morphologies. The first configuration (Figure 7(a)) consists in a perfectly plane contact interface, while the second involves an interface between a concave surface and a plane surface (Figure 7(b)). For the plane interface, the normal applied force will result in a quasi-uniform pre-stress. In this case, the interface will remain closed whatever the applied force. Conversely, for a concave interface, the central zone of the interface is initially open. Depending on the applied force, contact conditions will be changed, with the open part of the interface being gradually reduced from the sides to the center. For both cases (plane and concave interfaces), the interaction of the contact interfaces with a longitudinal wave is studied for different values of normal applied forces.

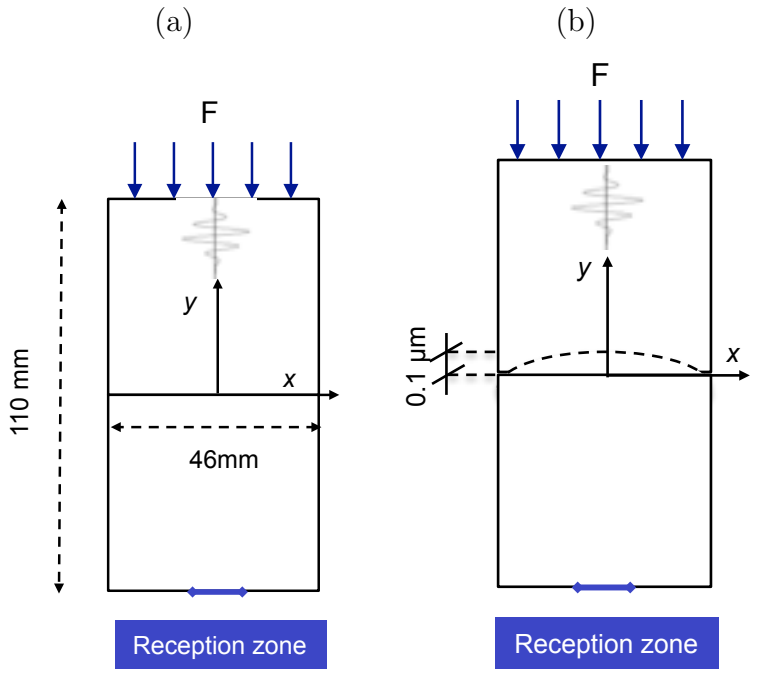

Figure 7: Schematic of the studied system : (a) perfectly plane interface and (b) concave interface on a plane interface including an open zone at the center and closed zones at either side.

4.1. Numerical modeling

PLAST2 is an explicit dynamic finite element code in 2D designed for large deformations and nonlinear material behavior [15]. It uses a forward Lagrange multiplier method for the contact between deformable bodies. For this dynamic study, the formulation is discretized spatially using a finite element method and discretized temporally by using a β_2 method. The contact algorithm uses slave nodes (located on the contact surface of the first block) and target surfaces (located on the contact surface of the second block) described by four node quadrilateral elements with 2×2 Gauss quadrature rule. Elementary target segments are described by two nodes and approximated by bicubic splines [16].

The contact dynamic generated along the contact interface is modeled by a unilateral contact with Coulomb's friction law, which gives the relations between contact stresses and displacements at the interface. Three states can be observed simultaneously at different nodes of the interface: "separation", "sliding" and "sticking". Switches between the different contact states introduce nonlinearity in the model. These boundary conditions can be referred to as non-smooth contact dynamics [17]. The top and bottom faces of the interface are denoted by $i = 1, 2$ respectively. Let $\boldsymbol{u}^i$ be the displacement and $\boldsymbol{n}^i$ the outward normal vector of face i of the crack, then the normal gap of displacements is defined by:

$$[u_n] = \boldsymbol{u}^1 \cdot \boldsymbol{n}^1 + \boldsymbol{u}^2 \cdot \boldsymbol{n}^2 = (\boldsymbol{u}^1 - \boldsymbol{u}^2) \cdot \boldsymbol{n}^1 \tag{5}$$

The incident wave creates stresses represented by the Cauchy stress tensor $\boldsymbol{\sigma}(\boldsymbol{u}^i)$. Denoting its normal component by $\sigma_n(\boldsymbol{u}^i)$ and its tangential component $\tau(\boldsymbol{u}^i)$, the unilateral contact

law is given by the following equation (similarly to equation 2):

$$\begin{cases} \sigma_n(\boldsymbol{u}^i) \leq 0 \\ [u_n] \leq 0 \\ (\sigma_n(\boldsymbol{u}^i)).[u_n] = 0 \end{cases} \tag{6}$$

Denoting the friction coefficient by μ and the tangential jump of displacements by $[u_t]$, the Coulomb's law is used to describe the tangential behavior:

$$\begin{cases} \mid \tau(\boldsymbol{u}^i) \mid \leq \mu \mid \sigma_n(\boldsymbol{u}^i) \mid \\ \text{If } \mid \tau(\boldsymbol{u}^i) \mid < \mu \mid \sigma_n(\boldsymbol{u}^i) \mid \Rightarrow \text{ sticking: } [u_t] = 0 \\ \text{If } \mid \tau(\boldsymbol{u}^i) \mid = \mu \mid \sigma_n(\boldsymbol{u}^i) \mid \Rightarrow \begin{cases} \text{sliding: } \exists \alpha \geq 0; [u_t] = -\alpha \tau(\boldsymbol{u}^i) \\ \tau(\boldsymbol{u}^i) = \pm \mu \mid \sigma_n(\boldsymbol{u}^i) \mid \end{cases} \end{cases} \tag{7}$$

In order to induce sliding, the shear stress $\mid \tau \mid$ has to be equal to $\mu \mid \sigma_n \mid$. When sliding occurs, the value of the shear stress depends on the global normal stress σ_n.

4.2. Numerical evolution of second harmonic efficiency as a function of the applied load

Calculations for each configuration and applied force values are performed in two steps. First, a normal force is applied. For the plane interface, it leads to a quasi-uniform pre-stress σ_0. For the concave interface, it leads to non-uniform distributions of pre-stress $\sigma_0(x)$ and initial gap $|u_0(x)|$ along the interface (Figure 8). Note that for a force greater than 1kN, the interface is completely closed.

In a second step, a longitudinal wave of five cycles is generated on the upper surface of the first block on a segment of 32 mm (diameter of experimental transducer) and propagates from top to bottom. The central frequency of this tone burst is 1 MHz and the displacement magnitude is set to u_{inc} =11 nm. The transducer of finite size generates a non-plane incident

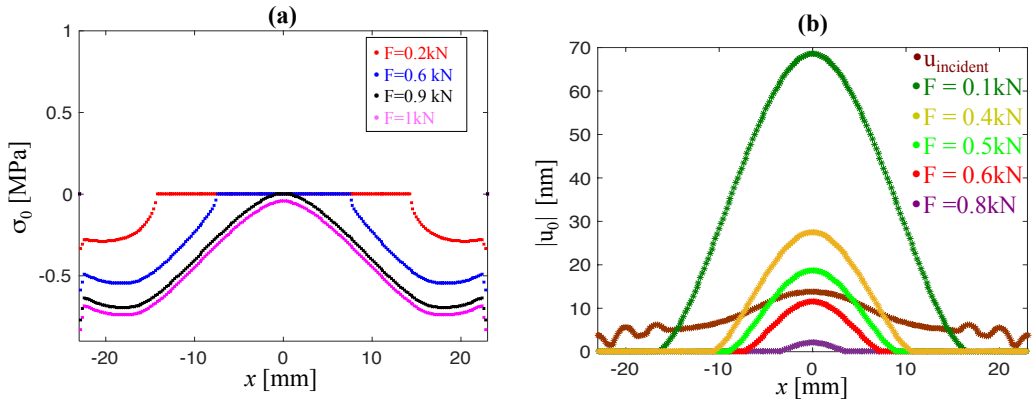

Figure 8: (a) Distribution of initial normal pre-stress $\sigma_0(x)$ along the contact interface and (b) initial normal gap for the concave interface for different normal forces.

wave. As a result, the distribution of the maximal normal stress associated with the incident wave at the interface is not uniform in the x-direction (as it can be seen in Figure 9).

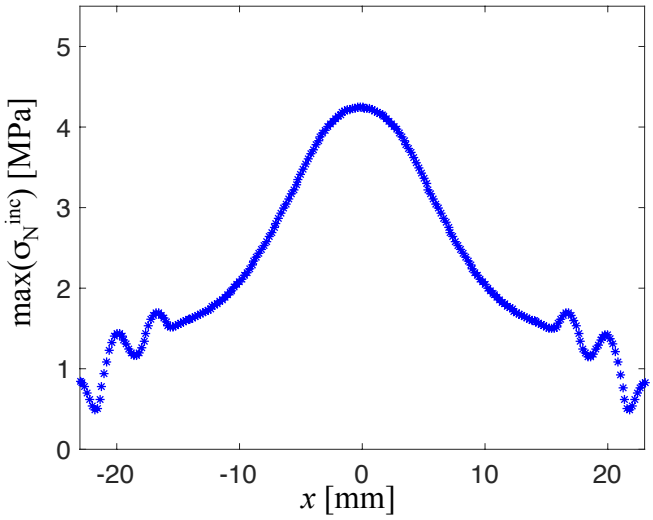

Figure 9: Distribution of the absolute value of maximal normal stress due to the incident wave at the interface. This distribution is obtained in the case of a perfect plane interface (continuity of stresses and displacements at the interface).

Normal velocity is recorded at the lower surface of the second block at each node of a segment of 10 mm. Measured signals are then summed and post-processed in order to extract the amplitude of the second harmonic A_2, as explained in section 2. Finally, numerical second

harmonic efficiency η_{num} is defined as the ratio of the second harmonic extracted from the integrated signal on the reception zone to the maximal value of the signal recorded at the interface in the case of a perfect plane interface(continuity of stresses and displacements at the interface). It is represented in Figure 10 as a function of the applied force for both interfaces morphologies. As expected, the evolution of η_{num} for the plane interface is similar to the evolution of a closed interface obtained previously. Nevertheless, the position of the maximum is slightly different due to the non-uniform distribution of incident normal stress. For the second configuration, although the evolution of η_{num} reaches a maximum for F $3.8kN$, it shows two slope discontinuities: one at $F \simeq 0.5\ kN$ and another at $F \simeq 1\ kN$. The evolution of this curve, including these two slope discontinuities, can be interpreted by a local contact analysis which is proposed in the following section.

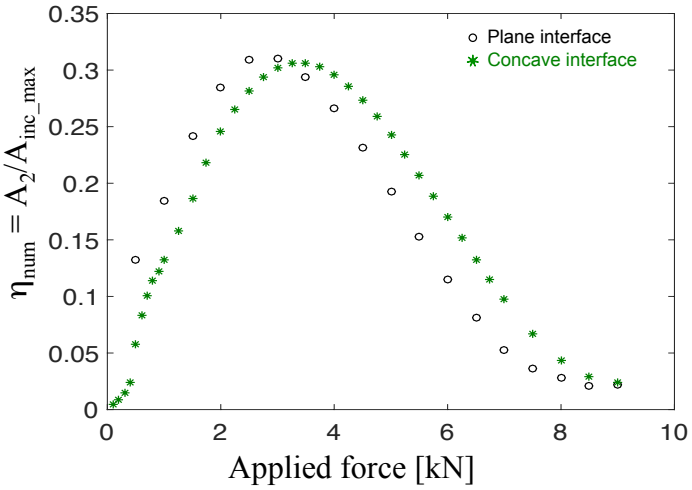

Figure 10: Numerical second harmonic efficiency η_{num} as a function of applied force for plane and concave interfaces. Numerical second harmonic efficiency is defined as the ratio of the second harmonic extracted from the integrated signal on the reception zone and the maximal value of signal recorded at the interface in the case of a perfect plane interface.

5. Local analysis of Contact Acoustic Nonlinearity and harmonic generation

In this part, a local analysis of CAN is proposed through local dimensionless parameters $\xi_L(x)$ and $\psi_L(x)$ along a contact interface defined as:

$$\xi_L(x) = \frac{|\sigma_0(x)|}{\sigma_{inc}^{max}(x)} \tag{8}$$

$$\psi_L(x) = \frac{|u_0(x)|}{u_{inc}^{max}(x)} \tag{9}$$

where $\sigma_{inc}^{max}(x)$ and $u_{inc}^{max}(x)$ correspond to maximal values of incident stress and displacement respectively. These parameters are dependent on x as the incident wave is non-plane (Figure 9), and the pre-stress and initial normal gap are non-uniform in the concave case (Figure 8). In the case of a plane interface, the initial gap is null and normal stress is constant along the interface. These parameters are introduced here in order to generalize the analysis provided by Richardson [9] and in section 2.

Case of plane interface. - Figure 11(b) shows the distribution of $\xi_L(x)$ along the interface for different load values. It is compared to the value of optimal $\xi_L^{opt} = 0.35$, which corresponds to a maximal value of second harmonic efficiency $\eta_{num} = A_2/A_{inc}$ in the case of a plane wave (presented in section 2). For a compression force of 3kN, $\xi_L \simeq \xi_L^{opt}$ at the center of the interface, the incident wave causes a maximum normal stress at the interface. This leads to a maximal value of second harmonic efficiency η_{num} (Figure 10). From a compressional force of 8.5 kN (not plotted), $\xi_L(x) > 1$ everywhere at the interface, indicating that "clapping" is not activated at the interface. Thus contact is permanent during wave transmission along the whole interface and $\eta_{num} \simeq 0$.

Figure 11(a) represents the distribution of the second harmonic efficiency $\eta(x) = A_2(x)/A_{inc}(x)$. For both configurations, particle velocities are recorded for each slave node of the interface

and band-pass filtered in order to extract the second harmonic amplitude $A_2(x)$. For an applied load of 2kN, the position of the maxima of $\eta(x)$ corresponds to the intersection between $\xi_L(x)$ and ξ_L^{opt}. For an applied load of 3 kN, $\eta(x)$ is maximal at the center of the interface, where $\xi_L(x) = \xi_L^{opt}$. Finally, for a load of 5kN, $\eta(x)$ decreases like $\xi_L(x) \leq \xi_L^{opt}$ along the whole interface. There appears to be a strong link between the distribution of second harmonic efficiency and the parameter $\xi_L(x)$.

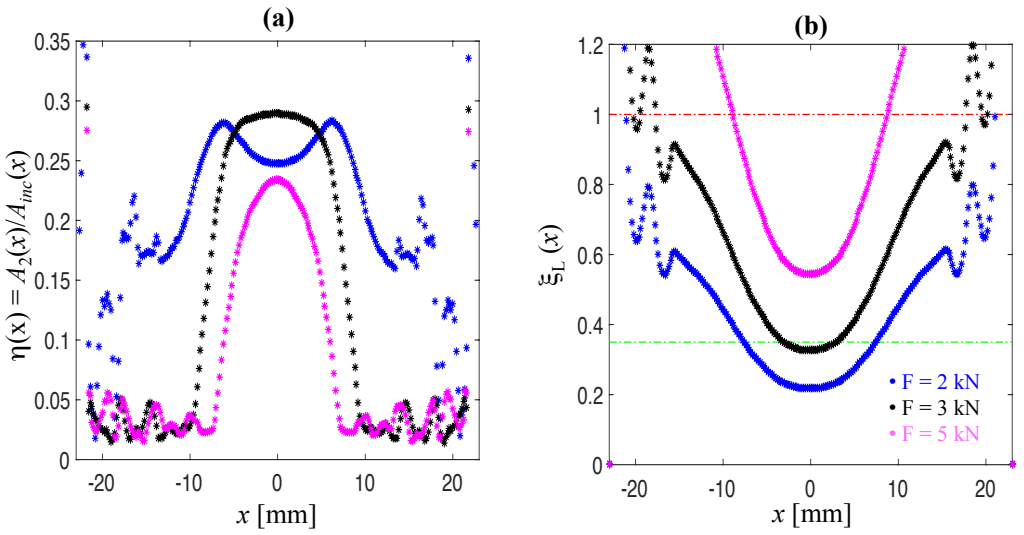

Figure 11: (a) Distribution of ratio $\eta(x) = A_2(x)/A_{inc}(x)$ for three different compression loads and (b) distribution of $\xi_L(x)$ along plane interface. Remarkable values for $\xi_L(x) = 1$ and $\xi_L(x) = \xi_L^{opt} = 0.35$ are represented by red and green lines respectively.

Case of concave interface. - As this interface contains *a priori* open and closed zones, two analyses are here necessary: one for the initially open zone using parameter $\psi_L(x)$ and one for the initially closed zone using the parameter $\xi_L(x)$. As shown in section 2, the second harmonic efficiency is greater for closed interfaces than for open ones. Moreover, nonlinear effects contribute more to the second harmonic efficiency when "clapping" is activated in the central zone than when it is at the edge of the interface due to the distribution of incident energy along the interface.

For the initially open zone, the nonlinear behavior of the interface is driven by parameter

$\psi_L(x)$ (Figure 12). For an applied load less than 0.4 kN, "clapping" is activated only in small zones at the edge of the interface. At the center of the interface, incident displacement amplitude is not sufficient to activate "clapping". Thus the contribution to η_{num} is weak. For an applied load of 0.5kN, "clapping" is activated along virtually the entire interface and η_{num} increases significantly. From an applied load of 1kN, the whole interface is closed and the nonlinear behavior is governed by $\xi_L(x)$. This corresponds to the second slope discontinuity in the variation of η_{num} in the case of a concave interface, observed in Figure 10.

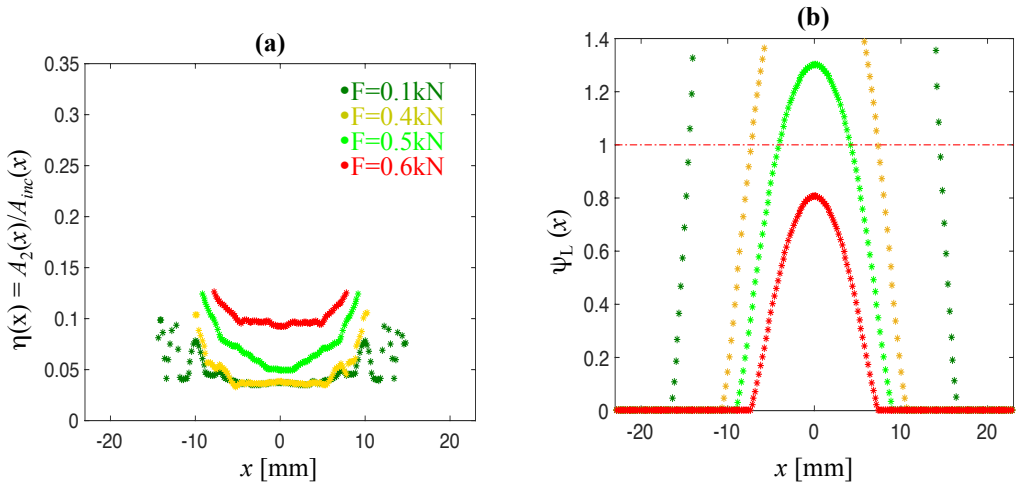

Figure 12: (a) Distribution of ratio $\eta(x) = A_2(x)/A_{inc}(x)$ for F=0.1 kN, 0.4 kN, 0.5 kN and 0.6 kN, in the open zone of the interface (for $|u_0| > 0$). (b) Distribution of $\psi_L(x)$ along the plane interface. $\psi_L(x) = 1$ is represented by a red line.

Figure 13(b) shows the distribution of $\xi_L(x)$ along the interface for three different applied loads. It can be seen that for an applied load of 3.5 kN, $\xi_L(x)$ reaches ξ_L^{opt} at the center of the interface, as was the case for the plane interface, resulting in a high value of η_{num}, close to the optimal value obtained for a force of 3.8 kN. For $F = 2$ kN, $\xi_L(x)$ reaches ξ_L^{opt} but in a zone where maximal incident normal stress is quite low (see Figure 9). Considering the case of a force of 5 kN, $\xi_L(x)$ is higher than ξ_L^{opt} everywhere on the interface, explaining why η_{num} is lower than for $F = 3.5$ kN. Considering the local distribution of $\eta(x)$, as for the plane interface, Figure 13(a) shows that it presents maxima where $\xi_L(x)$ reaches ξ_L^{opt}.

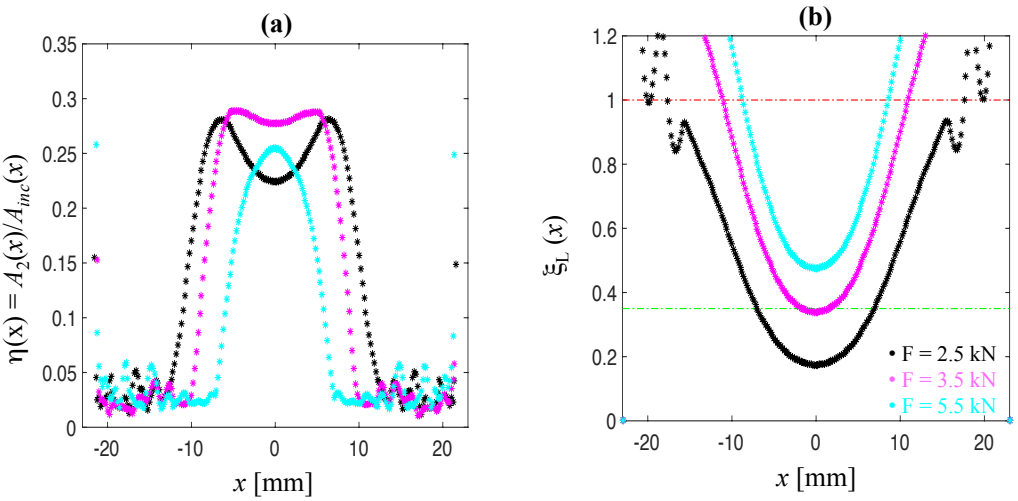

Figure 13: (a) Distribution of ratio $\eta(x) = A_2(x)/A_{inc}(x)$ for three different compression loads and (b) distribution of $\xi_L(x)$ along the concave interface. Remarkable values $\xi_L(x) = 1$ and $\xi_L(x) = \xi_L^{opt} = 0.35$ are represented in red and green lines respectively.

These results show that the distribution of $\eta(x)$ can be directly related to the distributions of $\psi_L(x)$ and $\xi_L(x)$. Thus this relation between these quantities suggests a strong potential for quantitative nondestructive evaluation of cracks or interfaces.

Figure 14 illustrates how the evolution of A_2 recorded at one point (here at the center of the interface) can be exploited. First, when $|u_0(0)| > u_{inc}$, the amplitude of the second harmonic is low. It increases significantly when $|u_0(0)| \simeq u_{inc}$. As the applied load is sufficient to close the interface, A_2 increases with a noticeable change of slope until a maximum reached for $F = 4$ kN. According to the analysis proposed above, the position of the maximum should correspond to $\xi_L(x) = \xi_L^{opt} = 0.35$. From this, if the incident wave amplitude were known, it would be possible to assess the pre-stress amplitude $|\sigma_0| = 0.35 * \sigma_{inc} = 1.48$ MPa. This calculated value is very close to the one recorded in the numerical simulation after stabilization of the first step of calculation (application of the normal load): $|\sigma_0(0)| = 1.45$ MPa. Thus, using the evolution of $A_2(x)$, some information about $u_0(x)$ and $\sigma_0(x)$ can be extracted. This is possible if the whole variation of the signature is available, if the

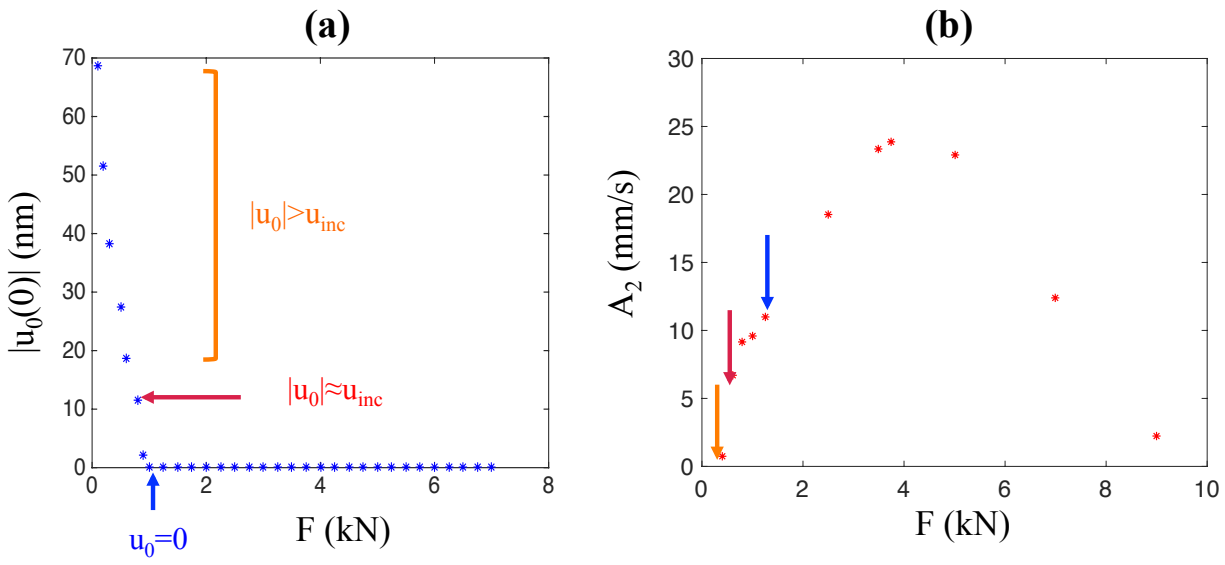

Figure 14: (a) Evolution of the gap at the center of the interface $|u_0(0)|$ and (b) Evolution of $A_2(0)$ as a function of normal force. The three arrows highlight the three forces identified in (a) where (from left to right) $u_0(x) > u_{inc}$, $u_0(x) \simeq u_{inc}$ and $u_0(x) = 0$.

incident magnitude is known and if contact behavior can be modeled by a unilateral contact law. It can be noted that there is an experimental issue for the assessment of $A_2(x)$ along the interface, as it is often a confined/internal zone. Nevertheless, solutions exist and can be used to evaluate $A_2(x)$ at the interface from measurements carried out at the surface of the solid blocks. This will be the subject of a future paper.

6. Conclusion

In this paper, the interaction of a longitudinal wave and a unilateral contact interface has been analyzed. First, a 1D analysis was carried out to retrieve evolutions of the second harmonic as a function of the dimensionless parameters ξ_L and ψ_L already described in the literature. These evolutions were compared to some experimental results in a sample with a real crack for different transmitter and receiver positions. These results motivated a 2-D FE analysis considering two blocks in contact with two different morphologies: a perfectly plane interface and a concave surface on a plane interface. By analyzing the local form

of the dimensionless parameters $\xi_L(x)$ and $\psi_L(x)$ the evolution of η_{num} and $\eta(x)$ could be explained. The link established in this paper between $\eta(x)$ and $\xi_L(x)$ and $\psi_L(x)$ can be exploited in view of a quantitative evaluation of interfaces or cracks (pre-stress, gap) under certain conditions. To apply this experimentally, a method needs to be developed where $\eta(x)$ can be assessed at the interface from measurements made far from the interface where it is possible and easy to measure signals. This will be the subject of a further paper.

Acknowledgments

The authors would like to thank Fondation CETIM for their support.

References

[1] Boris A. Korshak, I. Y. Solodov, and E. M. Ballad. Dc effects, sub-harmonics, stochasticity and "memory" for contact acoustic nonlinearity. *Ultrasonics*, 40:707–716, 2002.

[2] I. Y. Solodov, N. Krohn, and G. Busse. CAN: an example of nonclassical acoustic nonlinearity in solids. *Ultrasonics*, 40:621–625, 2002.

[3] C. Pecorari. Nonlinear interaction of plane ultrasonic waves with an interface between rough surfaces in contact. *Journal of the Acoustical Society of America*, 113(6):3065–3072, 2003.

[4] R. A. Guyer, K. R. McCall, and G. N. Boitnott. Hysteresis, discrete memory, and nonlinear wave propagation in rock: A new paradigm. *Phys. Rev. Lett.*, 74:3491–3494, Apr 1995.

[5] Maodan Yuan, Jianhai Zhang, Sung-Jin Song, and Hak-Joon Kim. Numerical simulation of rayleigh wave interaction with surface closed cracks under external pressure. *Wave Motion*, 57:143 – 153, 2015.

[6] P. Blanloeuil, A. Meziane, and C. Bacon. Numerical study of nonlinear interaction between a crack and elastic waves under an oblique incidence. *Wave Motion*, 51(3): 425 – 437, 2014. ISSN 0165-2125. doi: https://doi.org/10.1016/j.wavemoti.2013.10.002. URL http://www.sciencedirect.com/science/article/pii/S0165212513001613.

[7] Vladislav Aleshin, Steven Delrue, Andrey Trifonov, Olivier Bou Matar, and Koen Van Den Abeele. Two dimensional modeling of elastic wave propagation in solids containing cracks with rough surfaces and friction äì part i: Theoretical background. *Ultrasonics*, 82:11 – 18, 2018. ISSN 0041-624X. doi: https://doi.org/10.1016/j.ultras.2017.07.002. URL http://www.sciencedirect.com/science/article/pii/S0041624X17303694.

[8] Steven Delrue, Vladislav Aleshin, Kevin Truyaert, Olivier Bou Matar, and Koen Van Den Abeele. Two dimensional modeling of elastic wave propagation in solids containing cracks with rough surfaces and friction äì part ii: Numerical implementation. *Ultrasonics*, 82:19 – 30, 2018. ISSN 0041-624X. doi: https://doi.org/10.1016/j.ultras.2017.07.003. URL http://www.sciencedirect.com/science/article/pii/S0041624X17303700.

[9] John M. Richardson. Harmonic generation at an unbonded interface - I Planar interface between semi-infinite elastic media. *International Journal of Engineering Science*, 17 (1):73 – 85, 1979.

[10] B. O'Neill, R.G. Maev, and F. Severin. Distortion of shear waves passing through a friction coupled interface. In *Review of progress in Quantitative Nondestructive Evaluation*, volume 557, pages 1264–1267. AIP, 2001.

[11] O. Buck, W. L. Morris, and J. M. Richardson. Acoustic harmonic generation at unbonded interfaces and fatigue cracks. *Applied Physics Letters*, 33(5):371 –373, sep 1978.

[12] A. Meziane, A. N. Norris, and A. L. Shuvalov. Nonlinear shear wave interaction at a frictional interface: Energy dissipation and generation of harmonics. *Journal of the Acoustical Society of America*, 130(4):1820–1828, 2011.

[13] Maodan Yuan, Taekgyu Lee, To Kang, Jianhai Zhang, Sung-Jin Song, and Hak-Joon Kim. Absolute measurement of ultrasonic non-linearity parameter at contact interface. *Nondestructive Testing and Evaluation*, 30(4):356–372, 2015. doi: 10.1080/10589759.2015.1041523. URL `https://doi.org/10.1080/10589759.2015.1041523`.

[14] Philippe Blanloeuil, L.R. Francis Rose, Martin Veidt, and Chun H. Wang. Time reversal invariance for a one-dimensional model of contact acoustic nonlinearity. *Journal of Sound and Vibration*, 394:515 – 526, 2017. ISSN 0022-460X. doi: https://doi.org/10.1016/j.jsv.2017.01.050. URL `http://www.sciencedirect.com/science/article/pii/S0022460X17300901`.

[15] L. Baillet and T. Sassi. Mixed finite element methods for the Signorini problem with friction. *Numerical Methods for Partial Differential Equations*, 22(6):1489–1508, 2006.

[16] L. Baillet and T.Sassi. Mixed finite element formulation in large deformation frictional contact problem. *Revue Européenne des Eléments Finis*, 14(2-3):287–304, 2005.

[17] M. Jean. The non-smooth contact dynamics method. *Computer Methods in Applied Mechanics and Engineering*, 177(3–4):235 – 257, 1999.